Bifunctional amyloid-reactive peptide promotes binding of antibody 11-1F4 to diverse amyloid types and enhances therapeutic efficacy

Jonathan S. Wall[a,b,1], Angela D. Williams[a], James S. Foster[a], Tina Richey[a], Alan Stuckey[b], Sallie Macy[a], Craig Wooliver[a], Shawn R. Campagna[c,d], Eric D. Tague[c], Abigail T. Farmer[c], Ronald H. Lands[a], Emily B. Martin[a], R. Eric Heidel[e], and Stephen J. Kennel[a,b]

[a]Department of Medicine, University of Tennessee Medical Center, Knoxville, TN 37920; [b]Department of Radiology, University of Tennessee Medical Center, Knoxville, TN 37920; [c]Department of Chemistry, University of Tennessee, Knoxville, TN 37916; [d]Biological Small Molecule Mass Spectrometry Core, University of Tennessee, Knoxville, TN 37916; and [e]Department of Surgery, University of Tennessee Medical Center, Knoxville, TN 37920

Edited by Christopher M. Dobson, University of Cambridge, Cambridge, United Kingdom, and approved October 5, 2018 (received for review March 29, 2018)

Amyloidosis is a malignant pathology associated with the formation of proteinaceous amyloid fibrils that deposit in organs and tissues, leading to dysfunction and severe morbidity. More than 25 proteins have been identified as components of amyloid, but the most common form of systemic amyloidosis is associated with the deposition of amyloid composed of Ig light chains (AL). Clinical management of amyloidosis focuses on reducing synthesis of the amyloid precursor protein. However, recently, passive immunotherapy using amyloid fibril-reactive antibodies, such as 11-1F4, to remove amyloid from organs has been shown to be effective at restoring organ function in patients with AL amyloidosis. However, 11-1F4 does not bind amyloid in all AL patients, as evidenced by PET/CT imaging, nor does it efficiently bind the many other forms of amyloid. To enhance the reactivity and expand the utility of the 11-1F4 mAb as an amyloid immunotherapeutic, we have developed a pretargeting "peptope" comprising a multiamyloid-reactive peptide, p5+14, fused to a high-affinity peptide epitope recognized by 11-1F4. The peptope, known as p66, bound the 11-1F4 mAb in vitro with subnanomolar efficiency, exhibited multiamyloid reactivity in vitro and, using tissue biodistribution and SPECT imaging, colocalized with amyloid deposits in a mouse model of systemic serum amyloid A amyloidosis. Pretreatment with the peptope induced 11-1F4 mAb accumulation in serum amyloid A deposits in vivo and enhanced 11-1F4–mediated dissolution of a human AL amyloid extract implanted in mice.

amyloidosis | 11-1F4 | p5+14 peptide | immunotherapy | peptope

The systemic amyloidoses are a group of complex diseases characterized by the aggregation of normally soluble proteins into insoluble fibrils that deposit within extracellular spaces in abdominothoracic organs, peripheral nerves, and vasculature (1). The relentless accumulation of amyloid, notably in the heart, nerves, and kidneys, leads to disruption of tissue architecture and ultimately loss of function. Additionally, the amyloid fibrils may be cytotoxic (2) or induce metabolic dysfunction (3). At present, more than 25 structurally and functionally diverse proteins have been identified as components of the fibrils found in pathologic amyloid deposits (4). The most common forms of systemic amyloidosis are associated with the deposition of fibrils composed of monoclonal Ig light chains (AL), WT or mutant transthyretin (ATTR), leukocyte chemoattractant protein 2 (ALECT2), and serum amyloid protein A (AA).

Clinical management of amyloid-related disorders focuses principally on inhibiting production of the amyloid precursor protein or reducing its concentration. This is achieved by using antiplasma cell chemotherapy and autologous stem cell transplantation for patients with AL (5), tetramer-stabilizing small molecules in patients with ATTR (6, 7), and antiinflammatory drugs for those with AA-associated amyloidosis (8). These approaches can effectively decrease the concentration of the amyloid precursor protein and thereby halt the progression of amyloid deposition; however, they do not directly facilitate removal of existing tissue amyloid deposits. ALECT2-associated amyloid, a recently described form of amyloidosis prevalent in the southwestern United States (9, 10), has no specific treatment regimen as yet.

To address the goal of removing systemic amyloid from affected organs, three amyloid-reactive monoclonal antibodies (mAbs) have been developed to opsonize the deposits and thereby facilitate their dissolution (11–13). In early clinical trials, these mAbs have proven beneficial in a subset of patients, evidenced by improvement of biomarkers of organ function and reduction in hepatic amyloid load. These studies validate the paradigm that mAbs, capable of binding and opsonizing amyloid deposits, can provide therapeutic benefit by inducing cell-mediated destruction of tissue amyloid. Unfortunately, none of these antibodies yielded clinical improvement in all patients, and two of the antibodies are restricted for use in only AL-associated patients (11, 12). One of these mAbs, designated 11-1F4 (also known as CAEL101), has been shown by PET/CT imaging to accumulate in abdominothoracic organs of patients with AL

Significance

Amyloidosis is characterized by the deposition of pathologic protein fibrils in organs and tissues and is associated with ~25 disorders, including Alzheimer's disease and a systemic disease resulting from the aggregation of immunoglobulin light chains. Present treatments focus on reducing production of amyloid precursor proteins, but recent studies using amyloid-reactive antibodies have shown them capable of removing amyloid and improving organ function. To expand the utility of one such clinical antibody, designated 11-1F4, we have developed a synthetic, bifunctional peptide that binds many types of amyloid and mediates the recruitment of antibody to diverse amyloid types. This peptide approach may be used to enhance the efficacy and utility of existing antibodies, leading to broad-spectrum therapeutics and improved patient care.

Author contributions: J.S.W., A.D.W., J.S.F., and S.J.K. designed research; A.D.W., J.S.F., T.R., A.S., S.M., C.W., S.R.C., E.D.T., A.T.F., and S.J.K. performed research; J.S.W., J.S.F., R.H.L., E.B.M., R.E.H., and S.J.K. analyzed data; and J.S.W., J.S.F., R.H.L., E.B.M., R.E.H., and S.J.K. wrote the paper.

Conflict of interest statement: J.S.W., J.S.F., and S.J.K. are named inventors on a Patent Cooperation Treaty patent application that describes the use of peptope technology.

This article is a PNAS Direct Submission.

[1]To whom correspondence should be addressed. Email: jwall@utmck.edu.

This article contains supporting information online at www.pnas.org/lookup/suppl/doi:10.1073/pnas.1805515115/-/DCSupplemental.

Published online October 30, 2018.

amyloidosis (14). However, in this study only ∼65% of patients exhibited visual uptake of the mAb in organs, and accumulation in the heart and kidney was not readily demonstrable despite clinical manifestation of amyloid in these sites (14).

While these clinical data are promising, we continue to seek methods to improve the efficacy of existing antibodies for AL amyloid and provide a therapeutic adjunct that would allow treatment of multiple diverse forms of amyloid with a single opsonizing mAb. One approach is to explore the use of a two-step, pretargeting strategy (15, 16). To this end, we have developed a bifunctional, synthetic "peptope" that combines a multiamyloid-reactive peptide, designated p5+14, with a linear, high-affinity epitope of the 11-1F4 mAb. The p5+14 peptide is a 45-amino acid reagent comprising six amyloid-reactive heptad repeats (–KxxxKxx– where, x is Ala or Gln). It binds diverse types of amyloid-like fibrils, as well as human AL, ATTR, ALECT2, and AA amyloid in vitro and specifically colocalizes with systemic AA amyloid in a murine model of the disease (17–20). The peptide sequence was combined at the C terminus with a 12-amino acid linear peptide, designated A12, that binds the 11-1F4 mAb with subnanomolar affinity (21).

This peptope, designated p66 (Fig. 1*A*), is intended to expand the therapeutic utility of mAb 11-1F4 by serving as a multi-amyloid pretargeting reagent to facilitate opsonization by the 11-1F4 mAb (Fig. 1*B*); however, peptopes may be readily developed for other well-characterized mAbs. Herein, we describe in vitro binding studies using a panel of amyloid-like fibrils and human amyloid extracts, demonstrating that peptide p5+14 retains its amyloid reactivity in the context of the peptope. Similarly, we confirm the accessibility of the epitope for mAb binding when the peptope is bound to amyloid-like fibrils. Using a murine model of systemic AA-associated amyloidosis, we demonstrate in vivo binding of the peptope and its ability to mediate localization of murine 11-1F4 to AA amyloid deposits, a form of amyloid for which the antibody lacks significant inherent reactivity. Finally, we demonstrate enhancement of 11-1F4 mAb-mediated clearance of implanted human AL amyloid extract in a model of localized AL amyloid in the presence of peptope.

Results

Peptope p66 Retains both Epitope Binding and Multiamyloid Reactivity. Peptope p66 is a 63-amino acid polypeptide that was synthesized as a single product and purchased as a crude preparation that was purified using reverse-phase high-performance liquid chromatography (RP-HPLC). Purified p66 peptope eluting in peak one was used exclusively for these studies (*SI Appendix*).

The ability of murine (m) and chimeric (c) 11-1F4 mAbs to bind the A12 epitope in the context of peptope p66 was assessed by europium-linked immunosorbent assay (EuLISA). Both forms of 11-1F4 bound peptope p66 when surface adsorbed on a microplate well (Fig. 1*C*, black). The EC_{50} (midpoint of the binding transition) was estimated to be ∼0.4 nM, which was indistinguishable from the binding of 11-1F4 to the κ4 N-terminal peptide, LEN (1–22), derived from the Bence Jones protein LEN that served as the immunogen to generate m11-1F4 (Fig. 1*C*, gray). The binding of m- and c11-1F4 to surface adsorbed peptope p66 was not significantly inhibited by the presence of a 10- or 100-fold molar excess of p66 in solution (Fig. 1*D*). Both peptope p66 and peptide p5+14 were radioiodinated, and the binding to amyloid-like fibrils, human amyloid extracts, and AA-laden mouse liver homogenates was compared using a pulldown assay (Fig. 1 *E* and *F*). Experiments were performed either in PBS (Fig. 1*E*) or 1 M NaCl (Fig. 1*F*) to verify the importance of the electrostatic interactions between the peptides and the substrates. Both ^{125}I-p66 and ^{125}I-p5+14 peptides bound rVλ6Wil, Aβ (1–40), and human islet amyloid polypeptide (IAPP, associated with pancreatic islet amyloid in patients with type 2 diabetes) synthetic fibrils equivalently (Fig. 1*E*). Binding of ^{125}I-p5+14 to the human ALκ, ALλ, and ATTR amyloid extracts and murine AA liver homogenate was significantly greater (up to 20%) than that of ^{125}I-p66 (Fig. 1*E*). Neither peptide bound significantly to amyloid-free, WT mouse liver homogenate (∼10%) (Fig. 1*E*). In a milieu of 1 M NaCl, the reactivity of both radiolabeled peptides with amyloid extracts was dramatically decreased (≥60%); however, binding to the other substrates was unaffected by high salt (Fig. 1*F*).

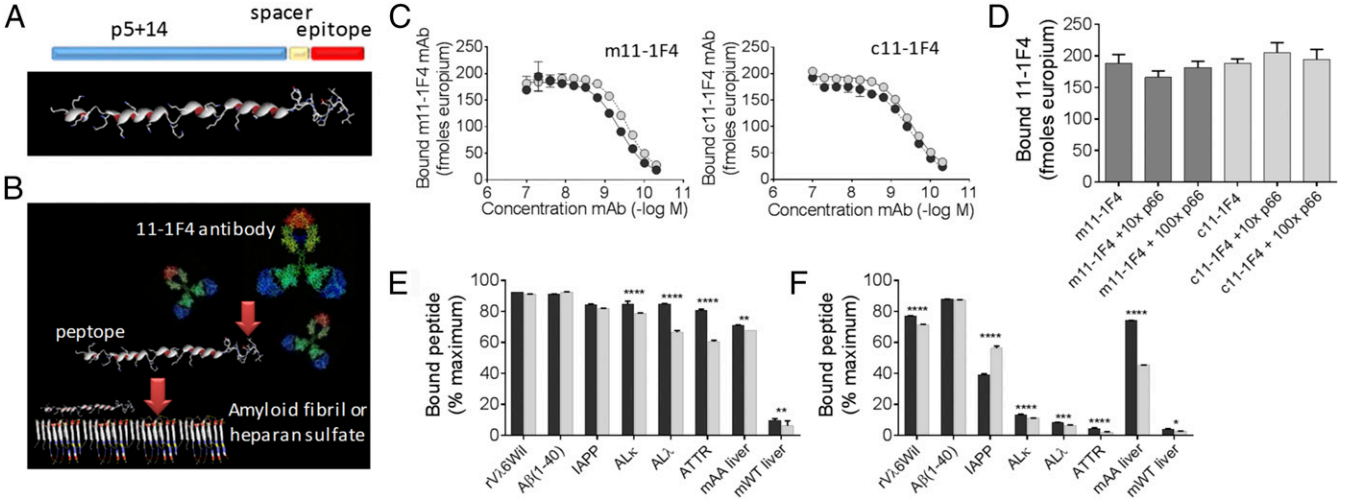

Fig. 1. Bifunctional peptope p66 binds diverse amyloids and mediates binding of mAb 11-1F4. (*A*) The p66 peptope comprises an amyloid-reactive peptide, p5+14, with a predicted helical secondary structure, coupled to a linear epitope bound by the 11-1F4 mAb. (*B*) Schematic representation of peptope pretargeting inducing the binding of 11-1F4 mAb to amyloid. (*C*) The m- and c11-1F4 mAb-bound surface adsorbed p66 (black; mean ± SD; $n = 5$) and the immunogen-derived peptide κ4Len (1–22) (gray; mean ± SD; $n = 5$) with similar subnanomolar affinity. (*D*) Murine and c11-1F4 preferentially bound surface adsorbed p66 even in the presence of 10× and 100× molar excess of p66 in solution. In pulldown assays, ^{125}I-p66 (black; $n = 3$) and ^{125}I-p5+14 (gray; $n = 3$) -bound synthetic amyloid fibrils, as well as human ALκ, ALλ, and ATTR amyloid extracts in PBS (*E*). Binding was reduced for both ^{125}I-p66 (black; $n = 3$) and ^{125}I-p5+14 (gray; $n = 3$) in 1 M NaCl (*F*) due to disruption of electrostatic interactions between p66 and the substrates. A two-way ANOVA with Sidak's multiple comparison test was used for statistical analysis in *E* and *F*, where, $^{*}P < 0.05$, $^{**}P < 0.01$, $^{***}P < 0.001$, $^{****}P < 0.0001$. Data are presented as mean ± SD.

Peptope p66 Specifically Binds Systemic AA Amyloid in Vivo. The tissue biodistribution of ^{125}I-p66 in vivo was studied in healthy mice as well as in a murine model of systemic amyloidosis in which severe AA-associated amyloid deposits occur in all abdominothoracic organs.

Organs were harvested, post mortem, at 1, 4, 24, and 72 h postinjection (h.p.i.) from mice administered ^{125}I-p66 and tissue-specific radioactivity measured (Fig. 2*A*). At 4 h.p.i. ^{125}I-p66 was observed at 5–7%ID/g (percent injected dose per gram tissue) in the liver, pancreas, and spleen, the major sites of amyloid deposition in the AA mouse. In contrast, <1%ID/g was observed in these organs of WT mice (Fig. 2*A*). Approximately, 4–7%ID/g was seen in the stomach of WT mice, reflecting uptake of free radioiodide liberated during renal catabolism of the peptide. At 24 h.p.i., the ^{125}I-p66 persisted in all organs and tissues of AA mice, compared with the WT mouse, with >4%ID/g present in the liver, pancreas, and spleen compared with <0.5% in WT mice (Fig. 2*A*). Small-animal, contrast-enhanced single-photon emission and X-ray computed tomography (SPECT/CT) imaging of representative mice administered ^{125}I-p66 was performed up to 72 h.p.i. Imaging data confirmed the presence of radioactivity persisting notably in the liver and spleen of AA mice (Fig. 2*B*).

The microdistribution of ^{125}I-p66 in vivo was visualized in murine organs at 4 and 24 h.p.i. by using microautoradiography, where binding of ^{125}I-p66 was evidenced by the presence black silver grains in the emulsion overlaying the tissues (Fig. 2*C*). At 4 h.p.i., dense deposits of ^{125}I-p66 were observed in each tissue that correlated precisely with the distribution of green-gold birefringent amyloid seen in Congo red-stained consecutive tissue

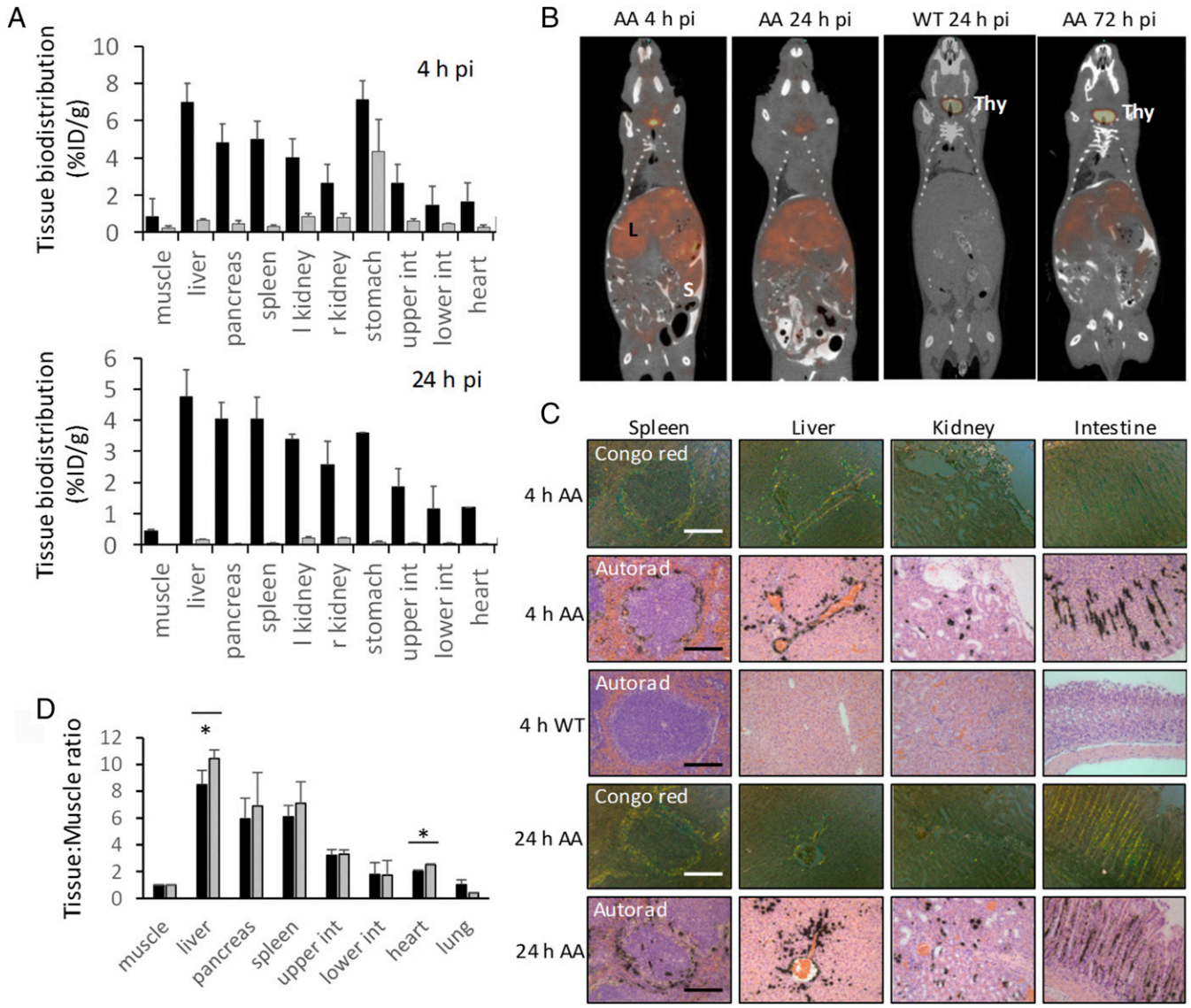

Fig. 2. Peptope p66 specifically binds amyloid in vivo and is comparable to peptide p5+14. (*A*) Biodistribution (%ID/g ± SD) of ^{125}I-p66 administered intravenously accumulated in organs and tissues of AA amyloid-laden H2/IL-6 mice (black; $n = 3$) but not amyloid-free mice (gray; $n = 3$) at 4 and 24 h.p.i. (*B*) SPECT/CT imaging revealed the presence of ^{125}I-p66 (false-colored red) in the liver (L) and spleen (S) of 2D-coronal images of AA-mice but not WT animals. Free radioiodide liberated during catabolism of the peptide was observed in the unblocked thyroid gland (Thy). (*C*) ^{125}I-p66 specifically bound amyloid deposits in tissues of AA-mice as evidenced by the presence of black silver grains in microautoradiographs (Autorad) that coincided with the distribution of birefringent amyloid in Congo red-stained consecutive tissue sections harvested from mice at 4 and 24 h.p.i. No ^{125}I-p66 was seen in organs of WT mice. (Scale bar, 250 μm.) (*D*) Dual energy tissue biodistribution measurements, expressed as tissue:muscle ratios of ^{125}I-p66 (gray; $n = 3$, mean ± SD) and ^{99m}Tc-p5+14 (black; $n = 3$, mean ± SD), administered concomitantly into AA mice revealed similar uptake in mice killed at 4 h.p.i. *$P < 0.05$.

sections (Fig. 2*C*). Notably, no binding of ^{125}I-p66 to amyloid-free tissue was seen in the AA mice or the WT animals. Binding of the radiolabeled peptope to amyloid persisted and was similarly amyloid-specific at 24 h.p.i. (Fig. 2*C*).

The in vivo amyloid reactivity of ^{125}I-p66 and ^{99m}Tc-p5+14 peptides was compared in individual AA mice (n = 3) by calculating dual-energy cross-over–corrected tissue:muscle ratio measurements (Fig. 2*D*). Both peptides accumulated similarly in the abdominothoracic organs of AA mice, notably in the liver, pancreas, and spleen; however, the ^{99m}Tc-p5+14 was significantly higher in the liver and heart tissues (Fig. 2*D*). These data confirm reactivity of p66 is comparable to that of the parent amyloid binding peptide p5+14.

Pretargeting of ^{125}I m11-1F4 mAb Using p66. The reactivity of m- and c11-1F4 mAbs to rVλ6Wil and Aβ (1–40) amyloid-like fibrils with and without pretreatment with p66 was used to assess the ability of peptope to enhance binding of the 11-1F4 mAb (Fig. 3 *A* and *B*). In the absence of p66, m11-1F4–bound rVλ6Wil (Fig. 3*A*, black) and Aβ (1–40) (Fig. 3*A*, gray) with estimated EC_{50} values of 45 nM and 140 nM, respectively. No binding of c11-1F4 to the amyloid-like fibrils was observed in this assay (Fig. 3*B*). In contrast, when the fibrils were preincubated with peptope p66, the binding of both m- and c11-1F4 was enhanced. The estimated EC_{50} for m11-1F4 binding to p66-treated rVλ6Wil and Aβ (1–40) fibrils increased to ∼0.6 nM (Fig. 3*A*). Similarly, the binding of c11-1F4 with pretreated fibrils was enhanced with EC_{50} values for rVλ6Wil and Aβ (1–40) fibrils of ∼0.6 nM (Fig. 3*B*). Similarly, the binding of radioiodinated m- and c11-1F4 mAb to human AL and ATTR amyloid extracts was enhanced 10- to 60-fold when the extract was pretreated with peptope p66 (Fig. 3 *C* and *D*). In these experiments, treatment of the amyloid extracts with peptide p5+14 served as a negative control.

Pretargeting of ^{125}I m11-1F4 mAb to AA Amyloid in Mice Using p66. The p66-mediated binding of m11-1F4 to human amyloid was further assessed ex vivo by using immunohistochemical staining (Fig. 3*E*). Pretreatment of formalin-fixed patient-derived tissue sections containing AA-, ATTR-, and AL-associated amyloid (selected as one of the amyloid samples that did not readily bind m11-1F4) with p66 resulted in m11-1F4 immunostaining that coincided with the presence of amyloid evidenced as green-gold

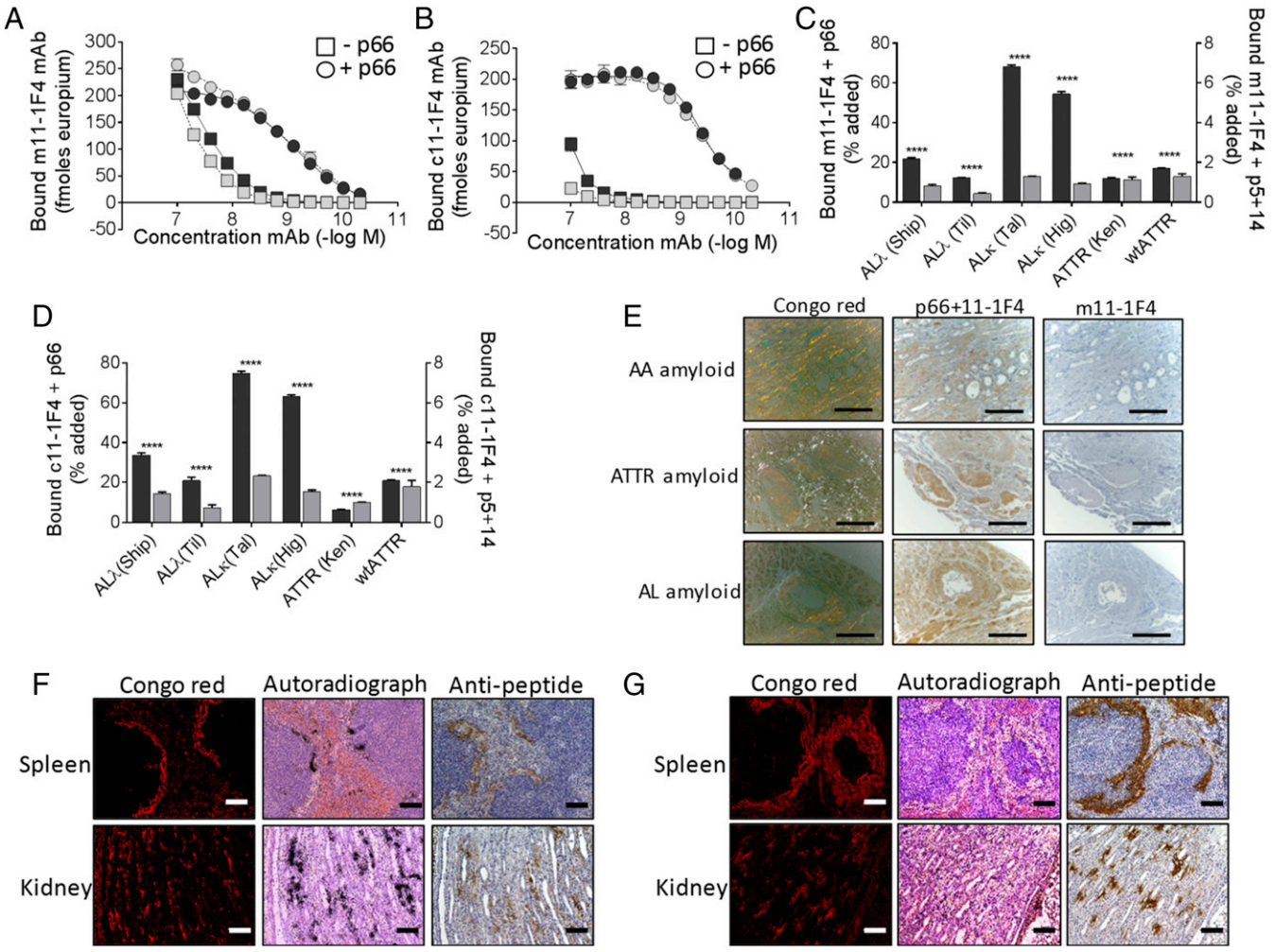

Fig. 3. Pretreatment of amyloid with p66 enhances binding of 11-1F4. Preincubation of rVλ6Wil (black; mean ± SD; n = 5) and Aβ (1–40) (gray; mean ± SD; n = 5) amyloid-like fibrils with p66 enhances the binding of m- (*A*) and c11-1F4 (*B*). Binding of ^{125}I-m11-1F4 (*C*) and ^{125}I-c11-1F4 (*D*) to human AL and ATTR amyloid extracts was enhanced by preincubation with p66 (black; n = 3; mean ± SD, left ordinate) but not peptide p5+14 (gray; n = 3; mean ± SD, right ordinate). (*E*) Treatment of human AA-, AL-, and ATTR-associated amyloid tissue sections with p66 promoted binding of m11-1F4 $F(ab)_2$ that coincided with the distribution of birefringent amyloid seen in Congo red-stained consecutive sections. (Scale bar, 250 μm.) Mice with AA amyloidosis were administered intravenously,(*F*) p66 (300 μg; n = 3) or (*G*) p5+14 (300 μg; n = 3) 24 h before intravenous injection of ^{125}I-m11-1F4. The mAb was retained in Congo red and p66^{+} amyloid as evidenced in autoradiographs, but not in the p5+14-treated mice. (Scale bars, 500 μm.) ****$P < 0.0001$.

birefringent material in Congo red-stained, consecutive tissue sections (Fig. 3*E*).

The 11-1F4 mAb does not exhibit significant binding to murine AA-associated amyloid. Therefore, we studied the ability of p66 pretreatment to facilitate uptake of ^{125}I-m11-1F4 by murine AA amyloid in vivo (Fig. 3 *F* and *G*). Mice with systemic AA amyloidosis were pretreated by an intravenous injection of 300 μg of p66 and 24 h thereafter administered ^{125}I-m11-1F4. The presence of ^{125}I-m11-1F4 associated with Congo-red staining amyloid in the spleen and renal papilla in p66-treated mice was evident by autoradiography (Fig. 3*F*) and colocalization of p66 with the amyloid was shown immunohistochemically using the 12-3 mAb (which does not bind AA amyloid) (*SI Appendix*, Fig. S3) in consecutive tissue sections (Fig. 3*F*). In contrast, ^{125}I-m11-1F4 did not bind to AA amyloid in mice administered the control peptide, p5+14, despite the presence of this peptide in the amyloid deposits as shown by immunohistochemistry (Fig. 3*G*).

Enhancing m11-1F4–Mediated Dissolution of Human Amyloid in Mice by p66 Pretreatment. We next questioned whether pretreatment of human AL amyloid extract with p66 could enhance 11-1F4–mediated amyloid dissolution in mice using a modification of the well-characterized subcutaneous amyloidoma model (22, 23). Female NU/NU mice (~8 wk of age) were injected subcutaneously on day 0 with 2 mg of human AL λ2BAL amyloid labeled covalently with Dylight800 (DL) NIR fluorophore and with (n = 5) or without (n = 4) preincubation in 200 μg of p66. Fluorescence emission from the subcutaneous amyloidoma was readily visualized on the flank of the mice by optical imaging (Fig. 4*A*). The rate at which the fluorescence emission, associated with the human amyloid extract, decreased was significantly enhanced in mice administered p66-pretreated material in response to m11-1F4 therapy, compared with m11-1F4 treatment alone (Fig. 4*B*). Using a mixed-effects analysis, we demonstrated a significant interaction between the p66 pretreated and 11-1F4 groups over the study period, $F(5, 40) = 6.46.$, $P < 0.001$, $\eta^2 = 0.45$, power = 0.99. Upon necropsy at day 17 postinjection, the residual amyloid appeared as a green mass intimately associated with the skin (Fig. 4*C*). Histologically, the amyloid mass was surrounded by fibroblast-like cells (Fig. 4*C*), retained its DL fluorescence, and was readily stained by Congo red (Fig. 4*C*). Infiltrating vasculature, evidenced by the presence of erythrocytes, was observed in the amyloidoma (Fig. 4*D*). Further immunohistochemical evaluation of the residual amyloidomas confirmed the presence of human λ LC$^+$ amyloid containing p66 peptide (in the pretreated mice) and m11-1F4 mAb (Fig. 4*E*). Macrophages immunostained with Iba-1–reactive antibody were observed predominantly at the periphery of the amyloidoma in p66-treated and untreated mice (Fig. 4*E*). The presence of macrophages and multinucleated giant cells with apparent intracellular amyloid were observed histologically in the p66-treated and untreated amyloid lesions (Fig. 4*F*). Immunohistochemical staining also demonstrated the absence of significant murine complement C3 in the amyloidoma (*SI Appendix*, Fig. S2).

In control studies, we ensured that the reduction of amyloid-associated fluorescence emission was not due to selective cleavage of the DL fluorophore from p66-pretreated amyloid. Formalin-fixed tissue sections containing the residual amyloid mass were stained with Congo red to ensure the presence of amyloid. A consecutive tissue section was then stained with thioflavin T (ThT),

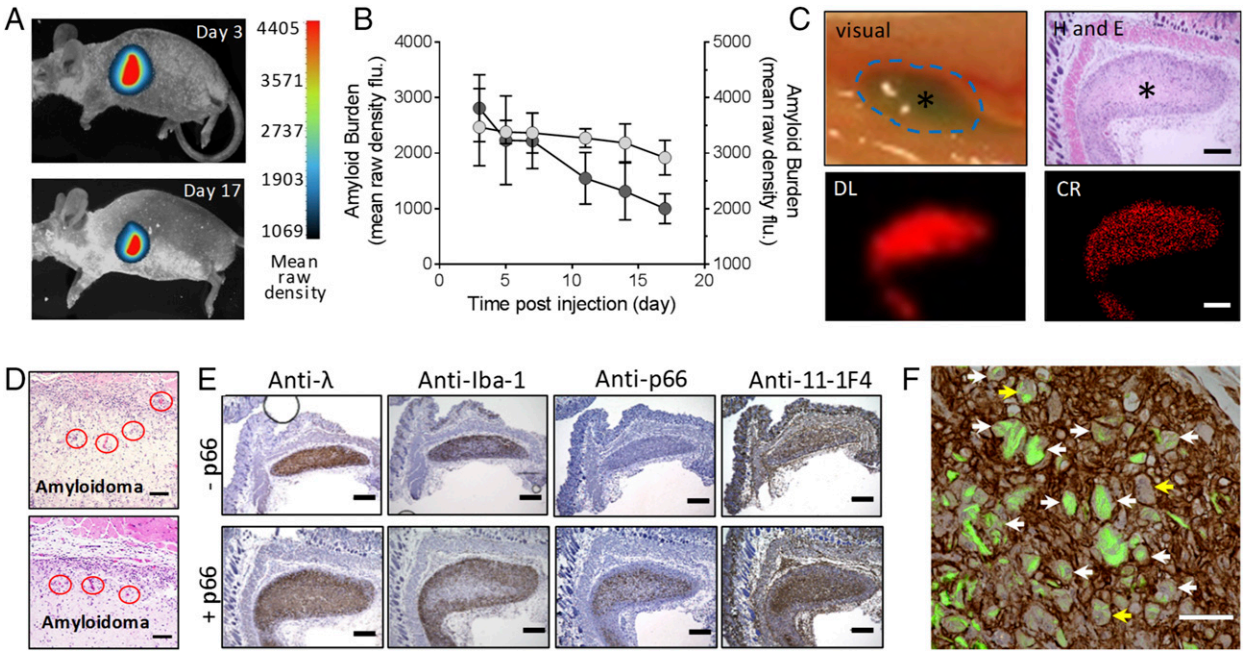

Fig. 4. Pretreatment of human amyloid extract with p66 enhances the therapeutic efficacy of 11-1F4 in mice. Female NU/NU mice were injected with 2 mg human λ2 amyloid extract [with 20% (wt/wt) DL-labeled amyloid] with (n = 5) or without (n = 4) pretreatment with p66, subcutaneously on the flank. (*A*) The fluorescence emission of subcutaneous amyloid extract was readily visualized by optical imaging. (*B*) Pretreatment with p66 enhanced the therapeutic activity of 11-1F4. Significant within-subjects [$F(5, 40) = 18.91$, $P < 0.001$, $\eta^2 = 0.70$, power = 1.00] and between-subjects [$F(1, 8) = 6.05$, $P = 0.039$, $\eta^2 = 0.43$, power = 0.58] effects were noted between p66-treated (dark gray, mean ± SD) and untreated mice (light gray, mean ± SD). Finally, a significant interaction was found between the groups in terms of rate of change across time, $F(5, 40) = 6.46.$, $P < 0.001$, $\eta^2 = 0.45$, power = 0.99. (*C*) In a representative case, the residual amyloid mass (asterisk) was associated with the skin, with a fibroblast layer encapsulating DL- and Congo red-positive amyloid material. (Scale bar, 500 μm.) (*D*) Representative images of residual amyloidoma revealing the presence of infiltrating vasculature (circles) in H&E-stained tissue sections. (Scale bar, 100 μm.) (*E*) The human amyloid mass immunostained positively for human λ light chains, Iba-1$^+$ macrophages, and 11-1F4 in both groups, and in the pretreated cohort, peptope p66 was observed. (Scale bar, 500 μm.) (*F*) Amyloidoma costained for Iba-1 (brown) and Congo red (false-colored green), multinucleated giant cells (yellow arrow) and macrophages were present with intracellular Congo red-positive amyloid (white arrows). (Scale bar, 50 μm.)

and the amyloid-associated ThT and DL fluorescence in the sections was quantified by optical imaging (Fig. 5*A*). The DL fluorescence intensity correlated positively with amyloid load, based on ThT fluorescence in the untreated and p66-treated samples (Fig. 5 *B* and *C*) and as a single population (Fig. 5*D*). No significant difference in the DL:ThT fluorescence ratio in the treated and untreated populations was observed (Fig. 5*E*), indicating that the reduction in DL fluorescence emission measured in vivo is associated with amyloid dissolution.

In light of the presence on macrophages in the subcutaneous λ2BAL amyloidoma, which may have taken up Congo red-positive amyloid by phagocytosis (Fig. 4*F*), we studied the effect of p66 treatment on m11-1F4–mediated phagocytosis of λ2BAL amyloid extract in vitro using cultured murine macrophages and amyloid labeled with a pH-sensitive fluorophore (*SI Appendix*, Fig. S4). Uptake of labeled λ2BAL amyloid into the acidified phagolysosme, where high fluorescence emission of pHrodo red is observed, was significantly greater in the presence of p66 and m11-1F4 compared with m11-1F4 alone and p5+14 with m11-1F4 (*SI Appendix*, Fig. S4). These data indicate that binding of m11-1F4 to the λ2BAL amyloid treated with p66 can significantly enhance phagocytosis by murine macrophages.

Discussion

Treatment of patients with systemic amyloidosis has long been challenging, with incremental but significant successes. There are currently two points of clinical intervention: (*i*) reducing production or availability of the amyloid precursor protein, and (*ii*) removal of deposits to allow recovery of organ function. Heretofore, treatment of amyloidosis has been dominated by the first of these approaches. Plasma cell-directed chemotherapy and autologous stem cell transplantation to suppress production of the amyloidogenic light-chain protein have been successful in stabilizing disease in many patients with AL-associated amyloidosis (24). Liver transplantation, and recently, gene silencing have been employed successfully to prevent hepatic production of amyloidogenic transthyretin (25). Drugs that stabilize the tetrameric form of transthyretin have been developed that prevent its dissociation into a monomeric component, thereby lowering the concentration of the amyloidogenic species and slowing further amyloid deposition (26). The use of antiinflammatory drugs, notably colchicine, to manage chronic inflammation reduces the production of the acute-phase reactant serum amyloid protein A, the precursor of AA-associated amyloidosis (27).

Despite these advances, most patients with peripheral amyloidosis present with clinically advanced disease at which time significant tissue amyloid has been deposited and organ damage is manifest. In almost all cases, a diagnosis of amyloidosis results, albeit belatedly, from symptoms of cardiomyopathy, renal insufficiency, or peripheral neuropathy (28, 29). For these patients, removal of amyloid deposits may stabilize or improve organ function. To this end, a new therapeutic paradigm has been developed for the treatment of patients with systemic amyloidosis; namely, the use of amyloid-directed passive immunotherapy using the humanized mAbs NEDO001 (12, 23, 30), dezamizumab (31), and the chimeric reagent 11-1F4 (11). All three mAb have demonstrated an excellent safety profile at the doses used (~15–24 mg/kg). Clinical evaluation of these mAbs has shown them capable of reducing amyloid load (13, 31) and improving surrogate biomarkers of cardiac and renal function (11, 30). Despite promising early-phase data from all these clinical trials, a recent placebo-controlled phase 2 clinical trial of mAb NEOD001 failed to meet primary outcomes, and the development of this drug was halted.

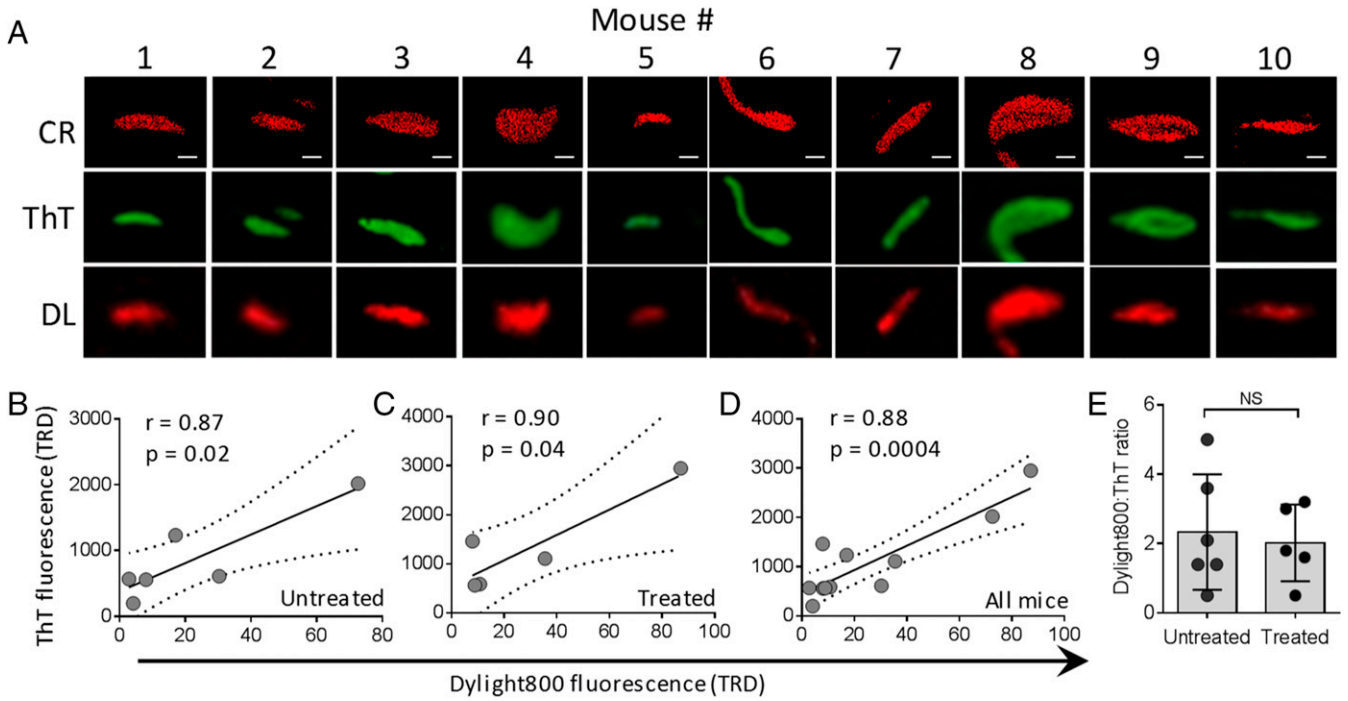

Fig. 5. In vivo amyloid fluorescence is surrogate for amyloid burden. (*A*) Residual amyloidomas from formalin-fixed paraffin-embedded tissues were imaged by fluorescence microscopy, following Congo-red staining, to identify the form of the amyloid deposit. A consecutive slide, stained with ThT, was imaged by using optical imaging with green fluorescence protein (GFP) and DL (NIR) filter sets. (Scale bars, 500 μm.) (*B*) The ThT and DL fluorescence images were quantified using a region of interest analysis and a Pearson correlation analysis performed between amyloid load, based on ThT fluorescence, and amyloid burden, based on DL fluorescence, for all amyloid samples for untreated (*B*), p66-treated (*C*), and all mice (*D*). (*E*)There was no significant difference in the DL:ThT ratio of the p66-treated and untreated cohorts. NS, not significant.

Passive immunotherapy of tissue amyloid is generally considered to rely on an interaction of mAb with the amyloid deposits, resulting in their opsonization and subsequent dissolution by phagocytic cells; however, of the clinically studied mAbs, only the m11-1F4 mAb has been shown by imaging to accumulate in amyloid-laden organs (14). In preclinical efficacy and mechanistic studies using a mouse model of inflammation-associated AA amyloidosis, the murine form of dezamizumab (an IgG2a) was shown to fix the complement C3 component and remove hepatosplenic amyloid deposits (32). The activation of macrophages and multinucleated giant cells was shown to be predominantly through the C3 receptor and not the FcR. The c11-1F4 mAb has also been shown to reduce amyloid load in a silver nitrate-induced model of murine AA amyloidosis (33). This reagent is capable of complement fixation, which may have contributed to the therapeutic effect, although direct binding to the amyloid deposits was not demonstrated, and the role of complement and macrophages was not investigated in this system. In contrast, the m11-1F4 mAb (IgG1κ) is unable to fix complement (34) and, therefore, likely activates innate immune cells via interactions with the FcR. In early studies of the m11-1F4–mediated dissolution of human AL amyloidomas in mice, it was shown that the circulating biological half-life of m11-1F4 was 164 ± 68 h (β-component of biexponential decay) in WT mice (35), which we anticipate will be similar in mice bearing a 2-mg human amyloidoma, given that the amount of target is so small. Additionally, it was shown granulocytes were critically involved, but no investigation into the role of macrophages was presented (22). Our data indicate that the binding of m11-1F4 to AA amyloid deposits is dramatically enhanced by pretreatment of the mice with p66 (Fig. 3 *F* and *G*); however, sufficient mAb may become amyloid-associated, after repeated injections of 5-mg/kg doses, to induce dissolution of AA amyloid (33).

The goal of the peptope technology is to generate an adjunct reagent that can be used in conjunction with these immunotherapeutics to enhance amyloid binding by coating the deposits with a high-affinity ligand. Additionally, it may be used to expand the utility of existing therapeutic mAbs for use in other less common forms of amyloidosis, thereby circumventing the need for specific mAbs for each form of amyloid, which number more than 25. These goals may be achieved by exploiting our multiamyloid-reactive, synthetic peptides that specifically target amyloid in vivo and can be used to deliver appropriate payloads to the deposits: in this case, a high-affinity linear epitope recognized by mAb (15, 16, 19).

The peptope concept and peptide p66 was developed to exploit the reactivity of peptide p5+14 with many diverse forms of amyloid (19). This peptide binds, via extensive electrostatic interactions, both the amyloid-associated heparan sulfate (as evidenced by its reactivity with heparin) and the proteinaceous fibrils (36). Electrostatic interactions have been shown to provide a basis for the reactivity of peptides and proteins with multiple diverse forms of amyloid-like fibrils (37–40). We have shown that polybasic peptides with a predicted α-helical or β-sheet secondary structure are reactive with ALκ, ALλ, ATTR, AA, ALECT2, Aβ (1–40), and IAPP fibrils or amyloid deposits (20, 41). Furthermore, these peptides did not bind to normal tissue in any assay tested in vitro or in mice. In conjunction with the peptide motif, we have utilized a linear high-affinity epitope recognized by m- and c11-1F4. For these studies, peptope p66 was synthesized from the C to N terminus as a single peptide using solid-phase FMOC synthesis. Due to the inherent inefficiency associated with synthesizing long peptides (42), multiple N-terminal truncated peptide species were present in the purified bioactive peak 1. Despite the loss of N-terminal glycine residues, the amyloid-reactive, polybasic heptad repeat region remained intact, and this allowed effective binding to amyloid-like fibrils (Fig. 1*C*) and human amyloid (Fig. 1*E*).

Pretargeting as a method for enhancing therapy is a well-established paradigm, exemplified by radioimmunotherapy of tumors using bispecific antigen-binding fragments [F(ab)] (43). As with all immunotherapeutic approaches, the target density, availability of the target to the vascular space, and the affinity of the interaction are all critical components that govern the efficacy of antibody uptake (44). Small synthetic peptides, as well as large multimeric proteins, such as SAP and mAbs, can rapidly accumulate in the amyloid compartment, which is readily available to the circulation as it serves as a source of the amyloidogenic precursor protein (14, 17, 45, 46). Ideal pretargeting of amyloid also requires that nonspecific binding to healthy tissues does not occur and that the unbound pretargeting agent is expeditiously removed from the circulation. We have shown that peptope p66 rapidly binds systemic AA amyloid in the mouse model (Fig. 2) and that the accumulation in organs and tissues is restricted specifically to the amyloid deposits where it is retained for >72 h. Within 24 h.p.i. in healthy mice, the major abdominothoracic organs contain <0.25%ID/g of radiolabeled p66. These properties are consistent with an effective pretargeting agent. Additionally, we have demonstrated that the presence of unbound peptope does not inhibit the binding of 11-1F4 mAb to amyloid-bound peptope (Fig. 1*D*), which may indicate that bivalent interactions of the mAb with surface-bound peptope effectively competes for monovalent interactions that may occur in the solution phase (e.g., circulation or extravascular fluid). This observation suggests that patients could be administered peptope injections even in the presence of circulating 11-1F4 mAb. Preclinical studies to evaluate strategies for effective clinical implementation of peptope as an adjunct to immunotherapy are underway.

Despite limited success (47–50), no experimental animal models of the most common forms of systemic amyloidosis in humans (AL-, ATTR-, and ALECT2-associated amyloidosis) recapitulate the complex pathology of the human conditions. In contrast, human IL-6–expressing transgenic mice, H2-L^{d}-huIL-6 BALB/c (H2/IL-6), develop severe abdominothoracic AA-associated amyloidosis reminiscent of patients with uncontrolled chronic inflammatory disorders (51, 52). Therefore, this model has been used extensively to study the in vivo targeting and specificity of multiamyloid peptides as an exemplar and surrogate for other forms of the disease (17, 19, 20, 53). Using these mice, we demonstrated that systemic pretreatment by intravenous administration of p66 effectively facilitated recruitment of m11-1F4 in AA-associated amyloid deposits (Fig. 3*F*), a form of amyloid for which 11-1F4 does not exhibit significant inherent reactivity. It is anticipated that, due to the multiamyloid-reactivity of p66, peptope reagents may be used to pretreat patients with diverse forms amyloidosis rendering them susceptible to dissolution mediated by 11-1F4 or other mAbs.

Due to the same limitations of experimental models of amyloidosis, we developed an iteration of the localized human AL amyloidoma mouse in which to test the effect of amyloid-bound p66 on 11-1F4 mAb-mediated amyloid dissolution in vivo (Fig. 4). In previous studies, 25–100 mg (dry weight) of human amyloid extract was implanted subcutaneously in mice and the mice manually palpated over ∼21 d to assess dissolution of the material, with the primary outcome measure being the wet-weight of the amyloidoma excised at necropsy. This model has been used to demonstrate targeting of agents to human amyloid and passive immunotherapy of human AL amyloid, by mAbs 2A4 (murine form of NEOD001) and m11-1F4, in the context of a complex biological system (22, 23, 54). However, due to the scarcity of human-derived amyloid material and the inability to quantitatively and longitudinally monitor amyloid resolution in vivo, we developed a model wherein as little as 2 mg of amyloid, labeled with a near-infrared dye and injected subcutaneously, could be readily measured noninvasively by optical imaging (Fig. 4). This model is suited for optical imaging techniques, because the amyloid is contained in the subcutaneous space such that

attenuation of the fluorescence emission is minimal. Our use of immunocompromised nude mice reduces autofluorescence from mouse hair, which can complicate quantitation of the emission signal, and ensures the absence of any specific endogenous adaptive immune response to the amyloid. Fluorescence associated with the amyloid material harvested at necropsy correlated directly with ThT staining of the mass in all mice, indicating that the fluorophore label was not selectively removed in mice treated with p66 and 11-1F4 mAb; thus, we could confidently ascribe fluorescence emission intensity with amyloid load (Fig. 5). Using this system, we were able to generate data amenable to a mixed-effect analysis, which demonstrated that 11-1F4 treatment of p66-coated λ2BAL amyloid extract was significantly more effective than 11-1F4 treatment alone, as evidenced by a more rapid decrease in amyloid-associated fluorescence in the lesion (Fig. 4). In these studies, macrophage infiltration and the presence of multinucleated giant cells were evidenced, and phagocytosis of the amyloid was observed in both $p66^{+}$ and $p66^{-}$ mice. We hypothesize that macrophage-mediated dissolution of amyloid is significantly enhanced when opsonization by m11-1F4 is increased by p66 pretreatment. This has been demonstrated in vitro using a phagocytosis assay employing the pH-sensitive fluorophore pHrodo red that is highly fluorescent in an acidic milieu, such as the macrophage phagolysosome (*SI Appendix*, Fig. S4). These data suggest that cell-mediated removal of tissue amyloid by 11-1F4, or other mAbs as part of a clinical immunotherapy approach, might be enhanced by pretargeting with an appropriate peptope even in patients where amyloid reactivity of the mAb is inherent, but insufficient.

In summary, the bifunctional peptope, p66, is a prototypic reagent that has been developed to enhance the immunotherapeutic efficacy of the mAb 11-1F4 in patients with AL-associated amyloidosis and expand its use to patients with other forms of amyloidosis. The peptope has been shown to bind many diverse forms of amyloid and, when used as a pretargeting agent, enhanced the accumulation of mAb 11-1F4 to amyloid deposits for which the mAb has no natural affinity. Pretreatment of human amyloid extract with p66 increased the rate of m11-1F4–mediated dissolution of the mass through phagocytosis of opsonized amyloid by infiltrating macrophages. This pretargeting approach may be amenable for use with any antibody having a known epitope structure, and may increase the immunotherapeutic options for patients with rare and diverse forms of amyloidosis.

Materials and Methods

Peptides and Antibodies. Peptide p5+14 (GGGYS KAQKA QAKQA KQAQK AQKAQ AKQAK QAQKA QKAQA KQAKQ) and the peptope, p66, (GGGYS KAQKA QAKQA KQAQK AQKAQ AKQAK QAQKA QKAQA KQAKQ SVTVV TKHYA AFPEN LLI) were purchased in crude form from Anaspec and were purified by RP-HPLC, as previously described (17), resulting in a single species on SDS/PAGE and HPLC with the predicted molecular weight of 4,766 Da. Peptope p66 resolved as two major peaks by RP-HPLC, and the composition of each peak was characterized by mass spectrometric analyses (*SI Appendix*). The recombinant λ6 variable domain (rVλ6Wil) was synthesized in *Escherichia coli* and purified, as previously described (55). Aβ (1–40) and human IAPP were purchased from Anaspec as 90% pure preparations and used without further purification for fibril synthesis. The Len (1–22) peptide (DIVMT QSPDS LAVSL GERAT IN) was purchased, as a >90% pure preparation, from Keck Small Peptide Synthesis Resource and used without further purification. The concentration of peptides and proteins were determined using a microBCA kit (ThermoFisher Scientific Pierce). Monoclonal antibody preparations m11-1F4 and c11-1F4 were prepared and supplied in sterile PBS by SAIC. The p5+14 and p66-reactive mAb, designated 12-3 (15), and the rabbit anti-idiotype antibody specific for 11-1F4 were generated and characterized in our laboratory.

Mass Spectrometry. Time-of-flight mass spectrometry using a Voyager-DE Pro Biospectrometry Workstation (Applied Biosystems) was employed to characterize the purified p66 components (*SI Appendix*).

Preparation of Fibrils and Amyloid Extracts. Amyloid-like fibrils composed of rVλ6Wil, Aβ (1–40) or human IAPP were prepared in PBS with 0.05% sodium azide and mouse liver homogenates were prepared from organs rich in AA amyloid or from WT animals, as previously described (36). Human amyloid extracts were prepared from autopsy-derived tissues from patients with AL (from patient samples λ2SHI, λ3TYL, λ2BAL, κ1TAL, and κ1HIG) or ATTR-associated amyloidosis using the water flotation method, as previously described (56). All animal studies described herein were carried out in accordance with protocols approved by the University of Tennessee Institutional Animal Care and Use Committee and in accordance with the guidelines provided by the Office of Laboratory Animal Welfare (OLAW) and the *Guide for the Care and Use of Laboratory Animals* (57). The University of Tennessee Graduate School of Medicine is an Association for Assessment and Accreditation of Laboratory Animal Care International (AAALAC)-accredited institutions. The use of human-subject–derived materials was approved by the University of Tennessee Graduate School of Medicine Institutional Review Board.

EuLISA. The binding of 11-1F4 mAb to peptope p66, Len (1–22) peptide, or amyloid-like fibrils was assessed by EuLISA. Peptides or fibrils were bound to high-binding 96-well microplates (Corning) by drying 50 μL of a 0.83 μM stock solution (in PBS) overnight at 37 °C. Nonspecific binding was then blocked by addition of 200 μL of PBS containing 1% BSA (PBSA) per well for 1 h at 37 °C. The 11-1F4 mAbs suspended in PBS with 1% BSA and 0.05% tween 20 (BSAT) were added to the wells, in triplicate with a 1:2 dilution, starting at 100 nM and incubated at 37 °C for 1 h. After washing unbound mAb from the wells, either biotinylated mouse or human Ig reactive polyclonal antibodies (Sigma-Aldrich) diluted 1:3,000 in BSAT were added and incubated for 1 h, 37 °C. Bound 11-1F4 was quantified by measuring time-resolved fluorescence using a Wallace Victor 3 plate reader (Perkin-Elmer) after serial addition of europium-conjugated streptavidin (1:1,000 dilution in BSAT, 1 h at room temperature; Perkin-Elmer) and 100 μL enhancement solution (1 h at room temperature; PerkinElmer).

Binding of 11-1F4 to amyloid-like fibrils was performed as described above, using 50 μL of 0.83 μM stock solution of fibrils in PBS to coat the microplate wells. In certain assays, the fibril-coated wells were treated with PBSA before preincubation with 100 μL of a 0.83 μM solution of peptope p66 for 1 h at 37 °C. The fibrils were then washed and the binding of mAb 11-1F4 and assessed as described above. For competition experiments, the 11-1F4 mAb (0.5 nM in PBS) was premixed with peptope p66 at 10- and 100-fold molar excess relative to the mAb concentration for 15 min before adding to the microplate well containing surface-adsorbed p66 peptope.

Protein Radiolabeling and Purification. Radiolabeling of p66, p5+14 or m11-1F4 mAb with ^{125}I or peptide p5+14 with ^{99m}Tc was performed as previously described (58). Briefly, peptides or antibodies (~50 μg) were added to 10 μL of 0.5 M sodium phosphate buffer pH 7.6 with ~2 mCi of ^{125}I (Perkin-Elmer) and 10 μg of chloramine T for 1–2 min at room temperature. The reaction was quenched by addition 10 μg of sodium metabisulfite and the products purified by gel filtration using a Sephadex G25 matrix (PD10; GE Healthcare) or Aca 34 resin (Sigma-Aldrich) with a mobile phase of 0.1% gelatin in PBS, pH 7.6. Column fractions corresponding to the radiolabeled protein were pooled and the products assayed for radiochemical purity by SDS/PAGE followed by phosphor image analyses. Retention of biological activity was assessed by pulldown assays using AA mouse liver homogenate (for peptides) or Len (1–22)-coated polystyrene beads (for 11-1F4). Peptide p5+14 was radiolabeled with ~2 mCi ^{99m}Tc (Cardinal health) in the pertechnitate form, using limiting amounts of $SnCl_2$. The radiolabeled peptide was purified and analyzed as described for the ^{125}I products above.

Pulldown Assays. The binding of radioiodinated peptides or 11-1F4 mAb with samples of synthetic amyloid fibrils, murine liver homogenates or amyloid extracts was performed using a pulldown assay, as previously described (19) and outlined in *SI Appendix*.

Histological and Immunohistochemical Tissue Staining. Formalin fixed paraffin-embedded canine (AA), and patient (AL and ATTR)-derived tissue sections were used to study the binding of m11-1F4. Tissue sections were subjected to antigen retrieval using citra-plus (Agilent-Dako). One set of tissue-sections was pretreated by addition of p66 peptope (3 μg/mL in PBS) overnight at 4 °C. Tissues were washed in PBS before addition of biotinylated m11-1F4 F $(ab)_2$ (0.1–0.5 μg/mL) in PBS at 4 °C overnight. The sections were again washed and avidin-biotin (ABC Elite kit; Vector) added for 60 min at room temperature before being developed using diaminobenzidene solution (ImmPACT DAB; Vector) for 3 min at room temperature.

Amyloid masses harvested from mice were immunostained for human λ light-chain– (1:20,000 dilution; Dako) or mouse-specific complement C3 (8 μg/mL; Santa Cruz Biological), following antigen retrieval by boiling in citrate buffer (Dako) for 30 min. Slides were developed by addition of peroxidase-conjugated anti-rabbit or anti-rat IgG (Vector) for 50 min at room temperature and DAB (as above). Macrophages were identified by first performing antigen retrieval using high pH target retrieval system (Dako) followed by staining overnight at 4 °C with Iba-1–reactive Ab (Wako Pure Chemicals) at a 1:9,000 dilution in antibody diluent (Dako) with background-reducing components (Dako). The secondary goat anti-rabbit IgG (Vectastain Kit; Vector Labs) and avidin-biotin conjugate (Vector) were each added for 30 min at room temperature before addition of DAB (Vector). In some cases, the Iba-1–stained tissue sections were counterstained using hematoxylin, eosin, and Congo red to reveal the presence of amyloid in the context of the macrophage staining. The presence of 11-1F4 was detected using an anti-idiotype rabbit polyclonal Ab (1 μg/mL) following antigen retrieval using glycine buffer (Glyca; BioGenex). Immunostaining of p66 and p5+14 peptide in mouse tissues was similarly performed using the biotinylated peptide-reactive mAb 12.3 (1.25 μg/mL in PBS).

Tissues were stained with alkaline Congo red solution 0.8% (wt/vol) Congo red, 0.2% (wt/vol) KOH (80% ethanol) for 1 h at room temperature followed by counterstain with Mayer's hematoxylin for 2 min, as previously described (17). ThT (Sigma-Aldrich) staining involved incubation in 1% (wt/vol) ThT for 3 min followed by 15 min in 1% glacial acetic acid. All tissue sections were counterstained with Gill Hematoxylin #3 (Sigma) by 30-s incubation at room temperature.

Photomicrographs were acquired using a Leica DM500 light microscope with a cooled CCD camera (SPOT RT-Slider; Diagnostic Instruments), fitted with cross-polarizing filters (for Congo red birefringence) or a BZ-X700E microscope (Keyence) fitted with a GFP (for ThT fluorescence), Texas red (for Congo red), and indocyanine green (for DL). Typically a 1/70- to 1/500-s or 1/2- to 1/15-s exposures were used for 4×- 20× objective brightfield and fluorescence images, respectively.

In Vivo Biodistribution and SPECT Imaging of ^{125}I-p66. AA amyloidosis was induced in the human interleukin 6 (huIL-6)-secreting transgenic H2-L^{d}-huIL-6 BALB/c (H2/IL-6) mice, as previously described (17). Mice with AA amyloidosis (4–6 wk postinduction) and healthy age-matched female WT animals were injected intravenously in the lateral tail vein with ^{125}I-p66 (~5 μg, ~100 μCi). After 1, 4, 24, and 72 h (no WT time point at 72 h due to lack of residual radioactivity at this time point), cohorts of three mice were killed by isoflurane overdose after receiving a 200-μL intraperitoneal injection of 10% Iohexol solution in PBS.

SPECT/CT images were acquired using an Inveon trimodality small-animal imaging system (Siemens Preclinical Solutions). SPECT images were generated by acquiring 60 64-s projections using 90 mm of bed travel with 1.5 revolutions. A 1.0-mm-diameter five-pinhole collimator was used and positioned at 30 mm from the center of rotation. Data were reconstructed using a maximum a priori 3D-ordered subset expectation maximization algorithm with 16 iterations and 6 subsets ($\beta = 1$). Images were displayed with 0.5-mm isotropic voxels on a matrix of 88 × 88 × 244 voxels. MicroCT data were acquired using an X-ray voltage biased to 80 kVp with a 500-μA anode current. A 240-ms exposure was used and 361 projections were collected covering 360° of rotation. The data were reconstructed using an implementation of the Feldkamp-filtered cone beam algorithm onto a 256 × 256 × 603 matrix with isotropic 211-um voxels with a bin factor of 4 and down-sampled by a factor of 2.

Following imaging, a necropsy was performed and the liver, heart, spleen, pancreas, left and right kidney, heart, lung, stomach, and upper and lower intestine harvested, placed in tared vials and the radioactivity measured using an automated Wizard 3 γ counter (1480 Wallac Gamma Counter; Perkin-Elmer). The biodistribution data were expressed as percent injected dose per gram tissue (% ID/g).

In Vivo Dual Energy SPECT Biodistribution Study in AA Mice. Dual-energy biodistribution studies were performed in a cohort of three H2/IL-6 mice at 4 wk postamyloid enhancing factor injection. Mice were injected intravenously in the lateral tail vein with a mixture of ^{125}I p66 (5 μg, 110 μCi) and ^{99m}Tc p5+14 (5 μg, 50 μCi) in a volume of 200 μL sterile PBS. At 4 h.p.i., the mice were killed, and a necropsy performed, as described above. Dual-energy tissue radioactivity measurements were performed using low- and high-energy windows for ^{125}I and ^{99m}Tc, respectively. A spillover correction for the low energy data of 9% was applied.

Autoradiography. Six-micrometer-thick sections were cut from formalin-fixed, paraffin-embedded blocks onto Plus microscope slides (Fisher Scientific), dipped in NTB-2 emulsion (Eastman Kodak), stored in the dark and developed after a 4-d exposure. Tissue sections were counter stained with hematoxylin. Tissues were examined microscopically and digital images acquired, as described above.

In Vivo Pretargeting of ^{125}I m11-1F4 in p66 Peptope-Treated Mice. Transgenic female H2/IL-6 mice were used at 3-wk postamyloid enhancing factor injection. A cohort of three H2/IL-6 mice and three WT mice were injected intravenously with 300 μg of either peptide p5+14 or peptope p66 in a 200-μL volume of sterile PBS. One day thereafter, the mice were administered ^{125}I m11-1F4 (~10 μg, 50 μCi) intravenously in the lateral tail vein, and 24 h thereafter, the mice were killed by isoflurane inhalation overdose and abdominothoracic organs harvested. The tissues were fixed in 10% buffered formalin for 24 h in preparation for microautoradiography and immunohistochemical staining. Tissue sections were imaged microscopically and digital images acquired, as described above.

Optical Imaging of Peptope-Enhanced Dissolution of Human Amyloid by mAb 11-1F4. Human λ2Bal AL amyloid extract was labeled with NHS-DL NHS-ester near-infrared dye (Thermo-Pierce) in 100 mM sodium bicarbonate buffer, pH 8.3 and the unbound dye removed by buffer exchange following centrifugation at 10,000 × *g* for 15 min. A cohort of NU/NU mice ($n = 5$) were administered subcutaneously 2 mg of λ2 amyloid containing 20% (wt/wt) DL-labeled extract pretreated with p66 (200 μg) in a volume of 0.2 mL of sterile PBS. A second cohort of mice ($n = 6$) received amyloid extract (20% DL) without pretreatment. Mice anesthetized by isoflurane inhalation were imaged using an iBox Scientia small animal optical imaging system (Analytik Jena) using a 800-nm bandpass filter (2-s exposure, 1 × 1 binning) and were treated by subcutaneous injection of 100 μg m11-1F4 at a contralateral site 6× over 17 d postinjection of the amyloid. Mice were killed by isoflurane overdose at day 17 postinjection and the residual amyloid masses harvested and fixed in 10% buffered-formalin.

ThT-stained slides containing λ2 amyloid extract excised from mice were imaged using the iBox Scientia small-animal optical imaging system with the GFP and NIR filter sets with a 0.5- and 2-s exposure, respectively.

In Vitro Phagocytosis Assay. The λ2BAL human AL amyloid extract was labeled with the pH-sensitive dye, pHrodo red-STP ester (Life Technologies), according to the manufacturer's instructions. Free pHrodo red dye was removed from the extract preparation by centrifugation at 2,000 × *g* for 15 min and washing in PBS. For the phagocytosis assay, ~1 × 106 RAW 264.7 cells (ATCC) were added to the center wells of a 24-well culture dish and cultured overnight in RPMI culture medium (Life Technologies) complete with 5% FCS, to form a monolayer.

Amyloid was prepared by taking 40 μg of λ2BAL (with 20% wt/wt pHrodo red-labeled extract) and mixing with 20 μg of peptide p5+14 (as a negative control) or p66 and the extract washed in PBS and recovered by centrifugation at 100 × *g*. The extract was then incubated in the presence of 60 μg of m11-1F4 or mAb 12–3 for 1 h at room temperature in PBS. The sample was then made to 1 mL with serum-free RPMI and added to the wells containing RAW 264.7 cells.

Following a 2.5-h incubation at 37 °C, the cells were imaged using a BZ-X700E microscope (Keyence) fitted with a Texas red filter. Four images of each well were acquired using a 4× objective lens, by an investigator blinded to the experimental conditions. Typically, a 0.5-s exposure was used for 4× fluorescence image capture. Image segmentation was performed using Image Pro Plus software and the area of red fluorescence measured and expressed per cell (phagocytosis) using the four low-magnification fields of view. Equivalent cell density was confirmed by Crystal violet staining.

Statistical Analyses. Skewness and kurtosis statistics were used to assess the normality of the data. Means and SDs were reported for the analyses. Analysis of pulldown assays was performed using a two-way ANOVA with Sidak correction for multiple comparisons. Pearson correlation analyses were performed using a two-tailed test with 95% confidence intervals plotted. Comparison of ^{125}I-p66 and ^{99m}Tc-p5+14 biodistribution in mouse tissues was performed by using a paired, two-tailed Student's *t* test. In vivo therapy data were analyzed using a mixed-effect ANOVA. Continuous observations were checked for normality using skewness and kurtosis statistics. Levene's Test for Equality of Variances was used to assess the assumption of homogeneity of variance. The assumption of sphericity was validated using Mauchly's test. The mixed-effects ANOVA was used to compare 11-1F4 treatment versus the 11-1F4 with p66 pretreatment in terms of fluorescence intensity across time. Between-subjects, within-subjects, and interaction effects were analyzed. Statistical significance was assumed at an α-value of 0.05. All statistical

analyses were performed using Prism software (v6.07; Graphpad Software) or SPSS v22 (IBM). Significance was set at $P < 0.05$.

ACKNOWLEDGMENTS. We thank Jim Wesley for assistance with tissue processing, sample preparation, and microautoradiography; and Matthew Little, who prepared the rVλ6Wil used in these studies. This work was supported by Public Health Service Grant DK110038 from The National Institute of Diabetes and Digestive and Kidney Diseases, as well as funds from the Molecular Imaging and Translational Research Program and the Department of Medicine at University of Tennessee Medical Center.

1. Wechalekar AD, Gillmore JD, Hawkins PN (2016) Systemic amyloidosis. *Lancet* 387: 2641–2654.
2. Marin-Argany M, et al. (2016) Cell damage in light chain amyloidosis: Fibril internalization, toxicity and cell-mediated seeding. *J Biol Chem* 291:19813–19825.
3. McWilliams-Koeppen HP, et al. (2015) Light chain amyloid fibrils cause metabolic dysfunction in human cardiomyocytes. *PLoS One* 10:e0137716.
4. Theis JD, et al. (2013) Proteome of amyloidosis in 4139 cases. *Blood,* 122:1900.
5. Chaulagain CP, Comenzo RL (2015) How we treat systemic light-chain amyloidosis. *Clin Adv Hematol Oncol* 13:315–324.
6. Bulawa CE, et al. (2012) Tafamidis, a potent and selective transthyretin kinetic stabilizer that inhibits the amyloid cascade. *Proc Natl Acad Sci USA* 109:9629–9634.
7. Coelho T, et al. (2013) Long-term effects of tafamidis for the treatment of transthyretin familial amyloid polyneuropathy. *J Neurol* 260:2802–2814.
8. Obici L, Merlini G (2012) AA amyloidosis: Basic knowledge, unmet needs and future treatments. *Swiss Med Wkly* 142:w13580.
9. Larsen CP, et al. (2016) Leukocyte chemotactic factor 2 amyloidosis (ALECT2) is a common form of renal amyloidosis among Egyptians. *Mod Pathol* 29:416–420.
10. Rezk T, et al. (2018) Diagnosis, pathogenesis and outcome in leucocyte chemotactic factor 2 (ALECT2) amyloidosis. *Nephrol Dial Transplant* 33:241–247.
11. Edwards CV, et al. (2017) Interim analysis of the phase 1a/b study of chimeric fibril-reactive monoclonal antibody 11-1F4 in patients with AL amyloidosis. *Amyloid* 24(sup1):58–59.
12. Gertz MA, et al. (2016) First-in-human phase I/II study of NEOD001 in patients with light chain amyloidosis and persistent organ dysfunction. *J Clin Oncol* 34:1097–1103.
13. Richards DB, et al. (2015) Therapeutic clearance of amyloid by antibodies to serum amyloid P component. *N Engl J Med* 373:1106–1114.
14. Wall JS, et al. (2010) Radioimmunodetection of amyloid deposits in patients with AL amyloidosis. *Blood* 116:2241–2244.
15. Wall JS, Foster JS, Martin EB, Kennel SJ (2017) Pretargeting immunotherapy: A novel treatment approach for systemic amyloidosis. *Pharm Pat Anal* 6:215–223.
16. Wall JS, et al. (2017) A bifunctional peptide, "peptope", for pre-targeting antibody 7D8 to systemic amyloid deposits. *Amyloid* 24(sup1):22–23.
17. Martin EB, et al. (2016) Comparative evaluation of p5+14 with SAP and peptide p5 by dual-energy SPECT imaging of mice with AA amyloidosis. *Sci Rep* 6:22695.
18. Wall JS, Kennel SJ, Martin EB (2017) Dual-energy SPECT and the development of peptide p5+14 for imaging amyloidosis. *Mol Imaging* 16:1536012117708705.
19. Wall JS, et al. (2015) Preclinical validation of the heparin-reactive peptide p5+14 as a molecular imaging agent for visceral amyloidosis. *Molecules* 20:7657–7682.
20. Wall JS, et al. (2011) In vivo molecular imaging of peripheral amyloidosis using heparin-binding peptides. *Proc Natl Acad Sci USA* 108:E586–E594.
21. O'Nuallain B, et al. (2007) Phage display and peptide mapping of an immunoglobulin light chain fibril-related conformational epitope. *Biochemistry* 46:13049–13058.
22. Hrncic R, et al. (2000) Antibody-mediated resolution of light chain-associated amyloid deposits. *Am J Pathol* 157:1239–1246.
23. Wall JS, et al. (2012) AL amyloid imaging and therapy with a monoclonal antibody to a cryptic epitope on amyloid fibrils. *PLoS One* 7:e52686.
24. Muchtar E, et al. (2017) Improved outcomes for newly diagnosed AL amyloidosis between 2000 and 2014: Cracking the glass ceiling of early death. *Blood* 129: 2111–2119.
25. Zimmermann TS, et al. (2017) Clinical proof of concept for a novel hepatocyte-targeting GalNAc-siRNA conjugate. *Mol Ther* 25:71–78.
26. Sultan MB, Gundapaneni B, Schumacher J, Schwartz JH (2017) Treatment with tafamidis slows disease progression in early-stage transthyretin cardiomyopathy. *Clin Med Insights Cardiol* 11:1179546817730322.
27. Oner A, Erdoğan O, Demircin G, Bülbül M, Memiş L (2003) Efficacy of colchicine therapy in amyloid nephropathy of familial Mediterranean fever. *Pediatr Nephrol* 18: 521–526.
28. Lousada I, Comenzo RL, Landau H, Guthrie S, Merlini G (2015) Light chain amyloidosis: Patient experience survey from the amyloidosis research consortium. *Adv Ther* 32: 920–928.
29. McCausland KL, et al. (2018) Light chain (AL) amyloidosis: The journey to diagnosis. *Patient* 11:207–216.
30. Gertz MA, Landau HJ, Weiss BM (2016) Organ response in patients with AL amyloidosis treated with NEOD001, an amyloid-directed monoclonal antibody. *Am J Hematol* 91:E506–E508.
31. Richards DB, et al. (2018) Repeat doses of antibody to serum amyloid P component clear amyloid deposits in patients with systemic amyloidosis. *Sci Transl Med* 10: eaan3128.
32. Bodin K, et al. (2010) Antibodies to human serum amyloid P component eliminate visceral amyloid deposits. *Nature* 468:93–97.
33. Solomon A, Weiss DT, Wall JS (2003) Therapeutic potential of chimeric amyloid-reactive monoclonal antibody 11-1F4. *Clin Cancer Res* 9:3831S–3838S.
34. Klaus GG, Pepys MB, Kitajima K, Askonas BA (1979) Activation of mouse complement by different classes of mouse antibody. *Immunology* 38:687–695.
35. Wall JS, et al. (2006) Radioimaging of light chain amyloid with a fibril-reactive monoclonal antibody. *J Nucl Med* 47:2016–2024.
36. Martin EB, et al. (2013) Peptide p5 binds both heparinase-sensitive glycosaminoglycans and fibrils in patient-derived AL amyloid extracts. *Biochem Biophys Res Commun* 436:85–89.
37. Habicht G, et al. (2007) Directed selection of a conformational antibody domain that prevents mature amyloid fibril formation by stabilizing Abeta protofibrils. *Proc Natl Acad Sci USA* 104:19232–19237.
38. Haupt C, et al. (2011) Pattern recognition with a fibril-specific antibody fragment reveals the surface variability of natural amyloid fibrils. *J Mol Biol* 408:529–540.
39. Haupt C, et al. (2011) Amyloid fibril recognition with the conformational B10 antibody fragment depends on electrostatic interactions. *J Mol Biol* 405:341–348.
40. Maderna E, et al. (2018) In situ tissue labeling of cerebral amyloid using HIV-related tat peptide. *Mol Neurobiol* 55:6834–6840.
41. Wall JS, et al. (2017) Specific amyloid binding of polybasic peptides in vivo is retained by beta-sheet conformers but lost in the disrupted coil and all D-amino acid variants. *Mol Imaging Biol* 19:714–722.
42. Katayama H, Nakahara Y, Hojo H (2011) N-methyl-phenacyloxycarbamidomethyl (Pocam) group: A novel thiol protecting group for solid-phase peptide synthesis and peptide condensation reactions. *Org Biomol Chem* 9:4653–4661.
43. Green DJ, Press OW (2017) Whither radioimmunotherapy: To be or not to be? *Cancer Res* 77:2191–2196.
44. Walker AJ, et al. (2017) Tumor antigen and receptor densities regulate efficacy of a chimeric antigen receptor targeting anaplastic lymphoma kinase. *Mol Ther* 25: 2189–2201.
45. Hawkins PN, Pepys MB (1995) Imaging amyloidosis with radiolabelled SAP. *Eur J Nucl Med* 22:595–599.
46. Minamimoto R, et al. (2013) Re-evaluating the potentials and limitations of (99m)Tc-aprotinin scintigraphy for amyloid imaging. *Am J Nucl Med Mol Imaging* 3:261–271.
47. Mishra S, et al. (2013) Human amyloidogenic light chain proteins result in cardiac dysfunction, cell death, and early mortality in zebrafish. *Am J Physiol Heart Circ Physiol* 305:H95–H103.
48. Solomon A, Weiss DT, Pepys MB (1992) Induction in mice of human light-chain-associated amyloidosis. *Am J Pathol* 140:629–637.
49. Teng J, Turbat-Herrera EA, Herrera GA (2014) An animal model of glomerular light-chain-associated amyloidogenesis depicts the crucial role of lysosomes. *Kidney Int* 86: 738–746.
50. Ward JE, et al. (2011) Metabolic phenotype in an AL amyloidosis transgenic mouse model. *Amyloid* 18(Suppl 1):40–41.
51. Solomon A, et al. (1999) Transgenic mouse model of AA amyloidosis. *Am J Pathol* 154: 1267–1272.
52. Wall JS, et al. (2008) Quantitative tomography of early-onset spontaneous AA amyloidosis in interleukin 6 transgenic mice. *Comp Med* 58:542–550.
53. Wall JS, et al. (2012) Comparative analysis of peptide p5 and serum amyloid P component for imaging AA amyloid in mice using dual-isotope SPECT. *Mol Imaging Biol* 14:402–407.
54. O'Nuallain B, Hrncic R, Wall JS, Weiss DT, Solomon A (2006) Diagnostic and therapeutic potential of amyloid-reactive IgG antibodies contained in human sera. *J Immunol* 176:7071–7078.
55. Wall J, et al. (1999) Thermodynamic instability of human lambda 6 light chains: Correlation with fibrillogenicity. *Biochemistry* 38:14101–14108.
56. Pras M, Schubert M, Zucker-Franklin D, Rimon A, Franklin EC (1968) The characterization of soluble amyloid prepared in water. *J Clin Invest* 47:924–933.
57. National Research Council (2011) *Guide for the Care and Use of Laboratory Animals* (National Academies Press, Washington, DC), 8th Ed.
58. Kennel SJ, Stuckey A, McWilliams-Koeppen HP, Richey T, Wall JS (2015) Tc-99m radiolabeled peptide p5 + 14 is an effective probe for SPECT imaging of systemic amyloidosis. *Mol Imaging Biol* 18:483–489.